EurJIC European Journal of Inorganic Chemistry

ChemPubSoc Europe

FULL PAPER

DOI:10.1002/ejic.201500050

Synthesis, Crystal Structures, Molecular Docking, and Urease Inhibitory Activities of Transition-Metal Complexes with a 1,2,4-Triazolecarboxylic Acid Derived Ligand

Yong-Peng Xu,[a] Yue-Hu Chen,[b] Zhi-Jian Chen,[a] Jie Qin,*[a] Shao-Song Qian,*[a] and Hai-Liang Zhu[a]

Keywords: Drug design / Inhibitors / Structure–activity relationships / Kinetics / Transition metals

Four novel complexes, $[Cu(\mathbf{L})_2(NH_3)_2(H_2O)_2]$ (**1**), $\{[Cu(\mathbf{L})_2(H_2O)_2]\cdot 2H_2O\}_n$ (**2**), $\{[Zn(\mathbf{L})_2(H_2O)_2]\cdot 2H_2O\}_n$ (**3**), and $\{[Fe(\mathbf{L})_2(H_2O)_2]\cdot 2H_2O\}_n$ (**4**) (H**L** = 2-{[4-amino-3-(pyridin-4-yl)-4,5-dihydro-1*H*-1,2,4-triazol-5-yl]thio}acetic acid) were synthesized and characterized by single-crystal X-ray diffraction analysis. Complex **1** exhibited a mononuclear structure. Complexes **2**, **3**, and **4** featured 2D networks. The crystal structures were stabilized by intermolecular hydrogen bonds to generate 3D supramolecular frameworks. The inhibitory activity was tested in vitro against jack bean urease. Among the four complexes, the two Cu^{II} complexes **1** and **2** exhibited better inhibitory activity than the positive reference acetohydroxamic acid, with IC_{50} values of 4.052 and 6.868 μM, respectively, whereas the Zn^{II} and Fe^{II} complexes showed no activity. To explore the mechanism of inhibition of the enzyme, kinetics studies were carried out; the results indicated that both the activated complexes **1** and **2** operated through a mixed-competitive inhibitory mechanism. Molecular docking was used to insert the most active complex **1** into the crystal structure of jack bean urease at the active site to determine the probable mode of binding.

Introduction

Urease (urea amidohydrolase, EC 3.5.1.5), a nickel-dependent metalloenzyme, exists in plants, animals, and bacteria with wide distribution in nature. Urease catalyzes the hydrolysis of urea into ammonia and carbon dioxide, and is responsible for providing organisms with a nitrogen source.[1] It is known to be one of the major causes of pathologies induced by *Helicobacter pylori* because it allows the bacteria to survive in the extreme acidic environment in the stomach and therefore could cause many gastroduodenal diseases such as gastritis, gastric and duodenal ulcers, and even gastric cancer.[2–7] A comprehensive report on the structure-based design and testing of a novel pharmacophore model for the recognition of urease inhibitors was envisaged by Zareen Amtul.[8] Based on their model, in our previous research, a 1,2,4-tiazole derivative **L1** (Scheme 1) and its complexes were investigated as urease inhibitors.[9] As a continuation of our work, we synthesized a modified triazole derivative H**L** (Scheme 1) (H**L** = 2-{[4-amino-3-(pyridin-4-yl)-4,5-dihydro-1*H*-1,2,4-triazol-5-yl]thio}acetic acid), in which the triazole nucleus was substituted with additional donor groups. This modification makes them very appealing for the design of new metal complexes with a broad spectrum of biological activities.[10]

In this research, we used the lead compound H**L** as a starting point for the design of more potent urease inhibitors. The ligand H**L** and a novel copper(II) complex, $[Cu(L)_2(NH_3)_2(H_2O)_2]$ (**1**), were synthesized and structurally characterized by single-crystal X-ray diffraction analysis. The use of molecular docking with Autodock 4.2 preliminary revealed that complex **1** exhibited potential urease inhibitory activities. The inhibitory activity was tested in vitro against jack bean urease and indicated complex **1** had better inhibitory activity than that of the positive reference acetohydroxamic acid. Structure-activity relationships[8] and the inhibitory efficiency of different transition-metal ions were considered in the present work. These were related to the observed pharmacological properties and used to determine the most important structure parameters controlling activity. Complexes $\{[Cu(\mathbf{L})_2(H_2O)_2]\cdot 2H_2O\}_n$ (**2**), $\{[Zn(\mathbf{L})_2(H_2O)_2]\cdot 2H_2O\}_n$ (**3**), and $\{[Fe(\mathbf{L})_2(H_2O)_2]\cdot 2H_2O\}_n$ (**4**) were synthesized, structurally characterized by X-ray diffraction, and evaluated in the urease inhibitory activities. In addition, we investigated the kinetics and mechanism of urease inhibition by complexes **1** and **2**; the results indicated that both complexes operated through a mixed-competitive

[a] School of Life Sciences, Shandong University of Technology, Zibo 255049, P. R. China
E-mail: sdutqianss@163.com
qinjietutu@163.com
http://www.sdut.edu.cn
[b] Research Institute of Nanjing University in Lianyungang, Lianyungang 222000, P. R. China

Supporting information for this article is available on the WWW under http://dx.doi.org/10.1002/ejic.201500050.

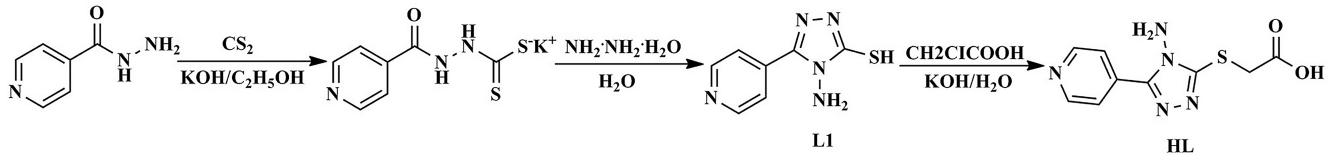

Scheme 1. Synthesis of ligand H**L**.

inhibitory mechanism. The computational predications showed good correlation with experimental data. The biological evaluation and mechanism study of complex **1** as a potent urease inhibitor is expected to be of significant interest.

Results and Discussion

Synthesis and Spectra

2-{[4-Amino-3-(pyridin-4-yl)-4,5-dihydro-1*H*-1,2,4-triazol-5-yl]thio}acetic acid (H**L**) was prepared in 63% yield. The ligand was stable and could be stored without special precautions. Generally, the ligand can dissolve in polar solvents such as methanol and *N*,*N*-dimethylformamide. Treatment of the ligand with metal salts $Cu(CH_3COO)_2{\cdot}H_2O$/$Zn(CH_3COO)_2{\cdot}2H_2O$/$FeCl_2$ with 1:1 molar ratio at ambient temperature led to formation of the complexes. Crystals of complexes that were suitable for X-ray diffraction could be isolated from methanol or *N*,*N*-dimethylformamide/methanol after slow evaporation of the solvent.

The broadness of the band at 3178–3311 cm^{-1} in the IR spectra of H**L** and complexes **1**–**4** can be attributed to a terminal NH_2 group and free water molecules.[11–13] Free H**L** shows a band at 1645 cm^{-1} attributable to the pyridyl ring vibrations. Upon pyridyl coordination to a metal, the band shifted to 1583–1591 cm^{-1},[14] which means that the ligand uses pyridyl nitrogen for chelate binding in complexes **1**–**4**. The IR spectrum of free H**L** contained two bands, $v_{as}(COO^-)$ located at 1578 and vs(COO^-) at 1388 cm^{-1}, which were attributed to the carboxyl group. The Δv value [$v_{as}(COO^-)$ – vs(COO^-)] was approximately 190 cm^{-1}, indicating a bidentate coordinating mode for the carboxylate group.[15] In complexes **2**–**4**, with bands at 1590 (or 1624, 1588) and 1356 (or 1381, 1365) cm^{-1}, the Δv values [$v_{as}(COO^-)$ – vs(COO^-)] were approximately 234 (or 243, 223) cm^{-1}, which can be assigned to the monodentate coordinated carboxyl.[15] These IR results were consistent with the crystallographic structural analyses.

Molecular Docking

To elucidate the interactions between the lead compound H**L** as a starting point for designing and identifying potential urease inhibitor agents, binding models of complex **1** with jack bean urease (3LA4) was simulated by using the Autodock 4.2 program to validate their structure-activity relationships. The results revealed that the target molecules fitted well in the active pocket of jack bean urease. Additional interactions were established in a variety of conformations because of the flexibilities of the amino acid residues of the urease. The optimized cluster (50 occurrences) was ranked by energy level in the best conformation of the inhibitor-urease modeled structures, and the binding energy of the amino acid residues with the corresponding copper(II) complex **1** showed –5.3 kcal/mol.

The binding model of complex **1** with urease (3LA4) is shown in Figures 1 and 2, with all the amino acid residues

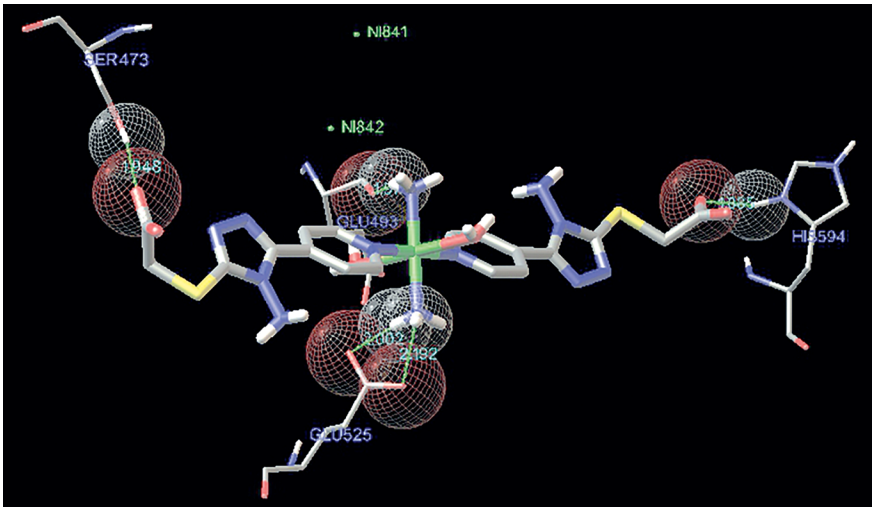

Figure 1. Modeled structures of complex **1** with jack bean urease.

that interact with urease indicated. In the binding model, complex **1** using the carbonyl oxygen as an acceptor received two hydrogen-bonding interactions from Ser473 and His594, with the distance of Ser473 N–H···O1 and His594 N–H···O2 being 1.948 and 1.885 Å, respectively. In addition, complex **1** bonded with the carboxylate group of Glu525 and Glu493, with hydrogen-bonding distances for N6–H6A···Glu525 O, N6–H6B···Glu525 O, and N6–H6C···Glu493 O being 2.192, 2.002, and 1.970 Å, respectively. In the inhibitor–urease complex conformation, complex **1** showed a stabilized structure through five hydrogen bonds with the carboxylate group and amino group of the amino acid residues. The results of the molecular docking indicated that complex **1** was well filled in the active pocket of jack bean urease.

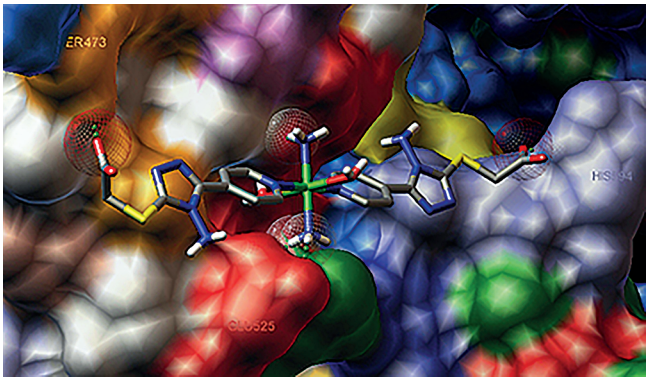

Figure 2. Binding mode of complex **1** with jack bean urease shown as a surface. Hydrogen bonds are presented as light-green dotted lines.

Crystal Structure Description of HL

The crystal data are shown in Table 1, and important bond lengths and bond angles of the complexes are summarized in Table 2.

Table 2. Selected bond lengths [Å] and angles [°] for complexes **1**, **2**, **3**, and **4**.

1		**2**	
Cu1–N1	2.038(2)	Cu1–N1A	2.0436(15)
Cu1–N6	2.0238(18)	Cu1–O2	1.9752(9)
Cu1–O1W	2.512(2)	Cu1–O1W	2.5741(10)
Cu1–N1A	2.038(2)	Cu1–N1B	2.0436(15)
Cu1–N6A	2.0238(18)	Cu1–O2A	1.9752(9)
Cu1–O1WA	2.512(2)	Cu1–O1WA	2.5741(10)
N1–Cu1–N6	88.86(7)	N1A–Cu1–O2	92.10(5)
N1–Cu1–O1W	92.46(8)	N1A–Cu1–O1W	98.30(5)
N1–Cu1–N1A	180.00	N1A–Cu1–N1B	180.00(8)
N1–Cu1–N6A	91.14(7)	N1A–Cu1–O2A	92.10(5)
N1–Cu1–O1WA	87.55(8)	N1A–Cu1–O1WA	81.71(5)
O1W–Cu1–O1WA	180.00	O1W–Cu1–O1WA	180.00
N6–Cu1–O1W	93.99(8)	O2–Cu1–O1W	94.51(3)
N6–Cu1–O1WA	86.01(8)	O2–Cu1–N1B	87.90(5)
N6–Cu1–N6A	180.00	O2–Cu1–O2A	180.00
3		**4**	
Zn1–N1	2.181(2)	Fe1–N1A	2.226(2)
Zn1–O1	2.0880(18)	Fe1–O2	2.0867(19)
Zn1–O1W	2.129(2)	Fe1–O1W	2.158(2)
Zn1–N1B	2.181(2)	Fe1–N1B	2.226(2)
Zn1–O1A	2.0880(18)	Fe1–O2A	2.0867(19)
Zn1–O1WA	2.129(2)	Fe1–O1WA	2.158(2)
N1–Zn1–O1	91.88(7)	N1A–Fe1–O2	92.00(8)
N1–Zn1–O1W	93.60(8)	N1A–Fe1–O1W	94.54(9)
N1–Zn1–N1B	180.00	N1A–Fe1–N1B	180.00
O1–Zn1–O1A	180.00	O2–Fe1–O2A	180.00
O1W–Zn1–O1WA	180.00	O1W–Fe1–O1WA	180.00
N1–Zn1–O1A	88.12(7)	N1A–Fe1–O2A	88.00(8)
N1B–Zn1–O1WA	86.40(8)	N1B–Fe1–O1WA	85.46(9)

Crystals of compound **HL** were obtained from methanol solution and characterized by single-crystal X-ray analysis. The crystal structure of **HL** is provided in the Supporting Information (Figure S1). **HL** crystallized in the monoclinic *C*2/*c* space group and the asymmetric unit contains one molecule. The ligand can act in polydentate mode through its pyridine nitrogen, hydrazine nitrogen, sulfur, and carboxyl group. The N1–N4 bond length of 1.404(7) Å is consis-

Table 1. Crystal data for compounds **HL**, **1**, **2**, **3**, and **4**.

	HL	**1**	**2**	**3**	**4**
Empirical formula	$C_9H_{10}N_5O_2SCl$	$C_{18}H_{26}N_{12}O_6S_2Cu$	$C_{18}H_{20}N_{10}O_6S_2Cu{\cdot}2H_2O$	$C_{18}H_{20}N_{10}O_6S_2Zn{\cdot}2H_2O$	$C_{18}H_{20}N_{10}O_6S_2Fe{\cdot}2H_2O$
Formula weight	287.74	634.20	636.16	638.00	628.46
Crystal system	monoclinic	triclinic	monoclinic	monoclinic	monoclinic
Space group	*C*2/*c*	$P\bar{1}$	$P2_1/c$	$P2_1/c$	$P2_1/c$
a [Å]	25.563(6)	7.1824(4)	10.8487(4)	10.9382(9)	10.9507(9)
b [Å]	7.5485(18)	7.5251(5)	14.6144(6)	14.7321(14)	14.7568(11)
c [Å]	13.310(3)	12.8134(7)	7.5686(3)	7.5831(6)	7.5408(6)
α [°]	90	78.885(2)	90	90	90
β [°]	110.231(7)	81.237(2)	90.100	90.907(2)	91.693(3)
γ [°]	90	62.587(2)	90	90	90
V [Å^3]	2409.0(10)	601.64(6)	1199.98(8)	1221.81(18)	1218.04(17)
Z	8	1	2	2	2
T [K]	273	293	293	273	273
$\rho_{calcd.}$ [g cm^{-3}]	1.586	1.750	1.761	1.734	1.714
F(000)	1184	327	654	656	648
μ (Mo-K_α) [mm^{-1}]	0.492	1.146	1.154	1.244	0.859
Theta min./max.	1.7/25.8	3.1/25.0	2.3/ 27.9	2.3/ 25.0	2.3/ 25.0
Final R_1,ωR_2 [$I > 2\sigma(I)$]	0.0857, 0.2313	0.0336, 0.0829	0.0324, 0.0870	0.0325, 0.0765	0.0406, 0.0887
Goodness of fit on F^2	1.06	1.09	1.05	1.05	1.03

tent with the reported value.[16] The C6–S1 bond length of 1.750(8) and C8–S1 bond length of 1.795(7) are longer than the reported C–S bond length of 1.693(2) Å. The C5–O2 bond length is also consistent with normal values, whereas the C5–O1 bond length is slightly longer than the theoretical value;[16] these results can be attributed to intermolecular hydrogen-bonding in the crystal (see Figures S2 and S3 in the Supporting Information).

Crystal Structure Description of $[Cu(L)_2(NH_3)_2(H_2O)_2]$ (1)

Complex **1** crystallized in the triclinic system $P\bar{1}$ space group. An ORTEP plot of complex **1** along with the atom numbering scheme is presented in Figure 3. Important bond lengths and bond angles of the complexes are shown in Table 2. The central Cu^{2+} ion, which lies on the inversion center, adopts a pseudo-octahedral coordination geometry that is defined by two nitrogen donors from two free ammonia and two oxygen donors from two coordinated water in the equatorial plane. The pyridyl nitrogen atoms from the ligand occupy the axial positions. The N1–Cu1–N1A bond angle of 180.00(11)°, clearly indicates that the three atoms are in a good linear configuration. The bond lengths of Cu1–N1 and Cu1–N6 are 2.038(2) and 2.0238(18) Å, respectively, which are consistent with the reported values.[17]

Hydrogen bonds for complex **1** are shown in Table 3. The adjacent molecules stack in a parallel arrangement. In the solid state, the mononuclear units are seized together forming a 2D network structure extended in the *ac* plane via N6–H6A···O1^{v}, O1W–H1WA···O1^{vi}, and O1W–H1WB···O2^{vii} (Figure 4) [symmetry codes: (v) 2 – *x*,1 – *y*,2 – *z*; (vi) 1 – *x*,1 – *y*,2 – *z*; (vii) *x*, –1 + *y*, –1 + *z*]. The crystal structure is also stabilized by N6 – H6B···O1^{vii} hydrogen bonds [symmetry codes: (vii) *x*, –1 + *y*, –1 + *z*], which link the 2D network into a 3D network (Figure 5).

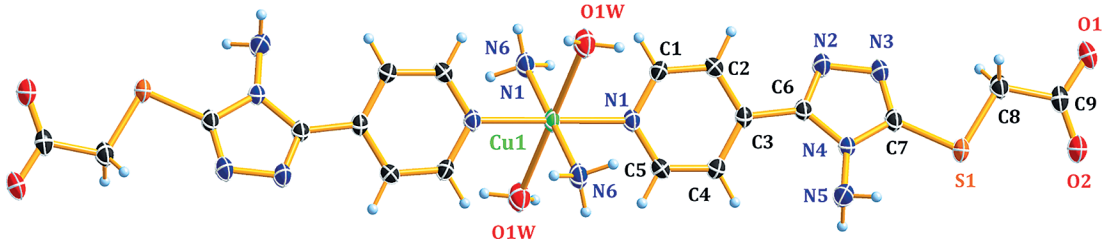

Figure 3. Crystal structure of complex **1**. Displacement ellipsoids are shown at the 50% probability level.

Table 3. Hydrogen bonds for complexes **1**, **2**, **3**, and **4** (Å).

Complex	D–H···A	*d*(D–H)	D(H···A)	*d*(D···A)	<(DHA)
1	N6–H6A···O1^{v}	0.92	2.08	3.007(3)	178
	O1W–H1WA···O1^{vi}	0.78(4)	2.05(4)	2.823(3)	178(4)
	O1W–H1W···O2^{vii}	0.85(4)	2.03(4)	2.872(3)	173(3)
	N6–H6B···O1^{vii}	0.92	2.39	3.283(3)	165
Symmetry codes: (v) 2 – *x*, 1 – *y*, 2 – *z*; (vi) 1 – *x*, 1 – *y*, 2 – *z*; (vii) *x*, –1 + *y*, –1 + *z*.					
2	O1W–H1W2···N3^{viii}	0.82	2.00	2.8123(18)	173
	O2W–H2W1···N2^{ix}	0.83	2.09	2.904(2)	167
	O2W–H2W2···O1^{x}	0.85	2.00	2.838(2)	169
	N5–H5A···O2W^{viii}	0.92	2.04	2.9549(15)	171
	N5–H5B···O2W^{viii}	0.91	2.12	3.0020(15)	162
Symmetry codes: (viii) *x*, 1/2 – *y*, –1/2 + *z*; (ix) 1 – *x*, –1/2 + *y*, 1/2 – *z*; (x) 1 + *x*, *y*, *z*.					
3	O1W–H1X···N3^{a}	0.74(4)	2.06(4)	2.794(3)	169(4)
	O2W–H2X···N2^{b}	0.87	2.02	2.891(3)	178
	O2W–H2Y···O2^{c}	0.84	2.04	2.872(3)	172
	N5–H5A···O2W^{d}	0.88(3)	2.18(3)	3.018(3)	160(3)
	N5–H5B···O2W^{e}	0.91(4)	2.08(4)	2.976(4)	170(3)
Symmetry codes: (a) *x*, 1/2 – *y*, 1/2 + *z*; (b) *x*, 3/2 – *y*, –1/2 + *z*; (c) 1 – *x*, 1 – *y*, 1 – *z*; (d) 2 – *x*, 1 – *y*, 1 – *z*; (e) 2 – *x*, –1/2 + *y*, 3/2 – *z*.					
4	O1W–H1W1···N5^{f}	0.85	1.92	2.769(3)	173
	N2–H2A···O2W^{g}	0.91	2.05	2.946(3)	168
	N2–H2B···O2W^{h}	0.99	2.11	3.030(3)	154
	O2W–H2W1···N4^{i}	0.847(13)	2.068(18)	2.894(3)	165(3)
	O2W–H2W3···O1^{i}	0.842(18)	2.020(18)	2.859(3)	174(4)
Symmetry codes: (f) *x*, 1/2 – *y*, 1/2 + *z*; (g) 1 + *x*, 1/2 – *y*, 1/2 + *z*; (h) 1 + *x*, *y*, *z*; (i) 1 – *x*, 1/2 + *y*, 3/2 – *z*.					

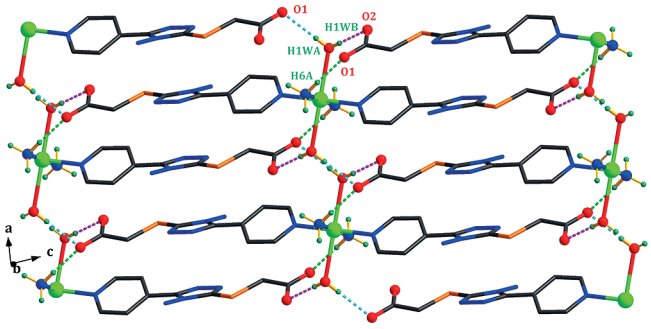

Figure 4. View of the 2D supramolecular sheet of **1**.

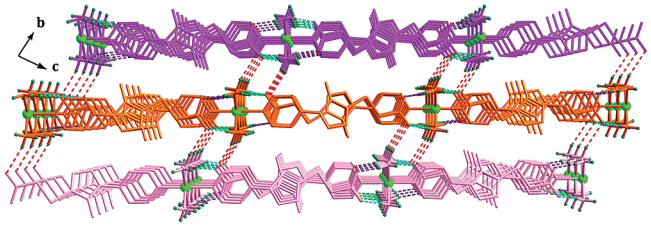

Figure 5. View of the 3D supramolecular sheet of **1** [symmetry codes: (v) 2 – *x*,1 – *y*,2 – *z*; (vi) 1 – *x*,1 – *y*,2 – *z*; (vii) *x*, –1 + *y*, –1 + *z*]. Hydrogen bonds are shown as dashed lines.

Crystal Structure Description of $\{[Cu(L)_2(H_2O)_2]\cdot 2H_2O\}_n$ (2)

Complex **2** crystallized in the monoclinic system $P2_1/c$ space group. As shown in Figure 6, the central Cu^{2+} ion adopts a pseudo-octahedral coordination geometry, which is defined by two nitrogen donors from two pyridine group in the axial positions, two oxygen donors from two coordinated water, and two oxygen donors from carboxyl groups in the equatorial plane. Selected bond lengths and angles of the complex are shown in Table 2. The difference between complexes **1** and **2** is that the carboxyl oxygen of **2** is involved in the coordination, resulting in a polymer structure.

As shown in Figure 7, complex **2** forms a 2D network supramolecular structure extended along the *ab* plane. The supramolecular network stack in a face-to-face fashion in

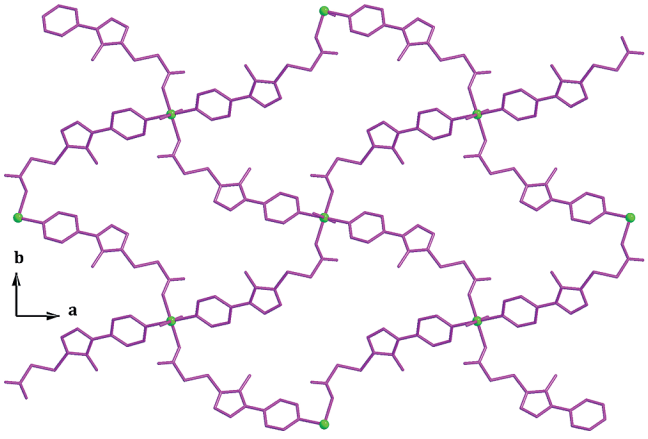

Figure 7. The 2D network structure of complex **2**.

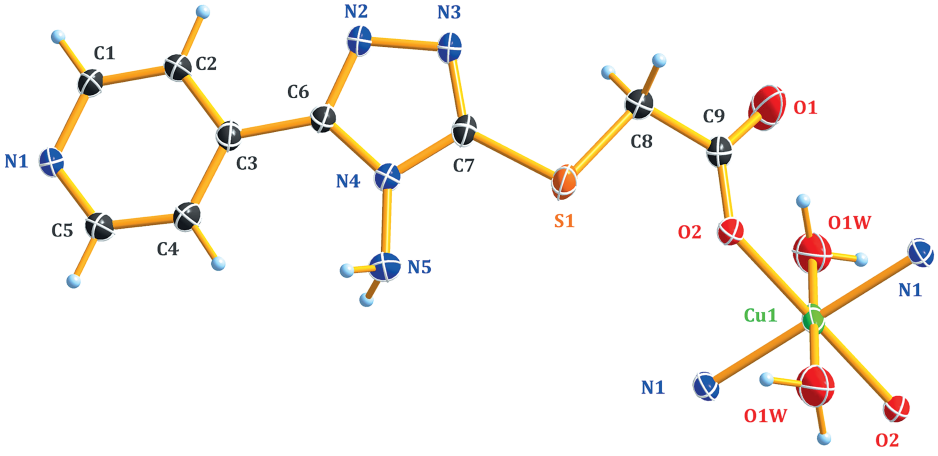

Figure 6. Crystal structure of complex **2** (50% thermal ellipsoids).

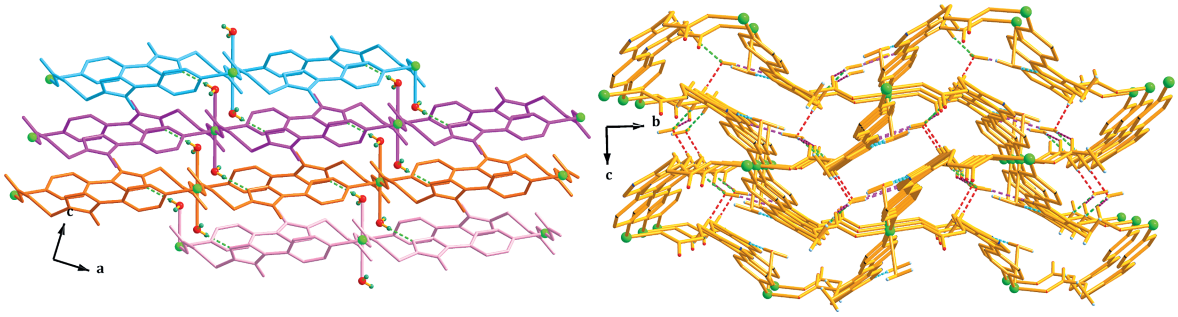

Figure 8. View of the 2D supramolecular sheet of **2** and 3D framework with hydrogen bonds indicated by dashed lines [(viii) *x*, 1/2 – *y*, –1/2 + *z*; (ix) 1 – *x*, –1/2 + *y*, 1/2 – *z*; (x) 1 + *x*, *y*, *z*].

the *ac* plane, the hydrogen bonds between the triazole nitrogen atoms from HL and the coordinated water form an intermolecular O1W–H1A2···N3^{viii} [symmetry code: (viii) x, 1/2 – y, –1/2 + z] hydrogen-bonding interaction, leading to the construction of a 2D supramolecular sheet in the *ac* plane (Figure 8). Complex **2** is stabilized by intermolecular hydrogen-bonds involving O2W–H2W1···N2, O2W–H2W2···O1, N5–H5A···O2W, and N5H5B···O2W forming the 3D supramolecular sheet (Figure 8). Hydrogen bonds for complex **2** are summarized in Table 3.

Crystal Structure Description of $\{[Zn(L)_2(H_2O)_2]\cdot 2H_2O\}_n$ (3)

X-ray crystallographic analysis revealed that the molecular structure of complex **3** crystallized in the monoclinic $P2_1/c$ space group. Similar to the crystal structure of complex **2** shown in Figure S4 in the Supporting Information, the central Zn^{2+} ion in **3** also lies on the inversion center and adopts a pseudo-octahedral coordination environment. The equatorial plane is surrounded by two O-atom donors from carboxyl groups and two O-atom donors from coordinated water molecules, whereas the axial positions are occupied by two nitrogen atoms from the triazole moiety of the ligand HL. Selected bond lengths and angles are shown in Table 2; hydrogen bonds are shown in Table 3. Given that complex **3** presents a structure that is similar to that of **2**, complex **3** is also a polymer structure and stabilized by the presence of the intermolecular hydrogen bonds (Figure S5, S6, and S7).

Crystal Structure Description of $\{[Fe(L)_2(H_2O)_2]\cdot 2H_2O\}_n$ (4)

Complex **4** crystallized in the monoclinic system $P2_1/c$ space group. The crystal structure of **4** is similar to those of **2** and **3**, with the central iron ion also adopting a pseudo-octahedral coordination geometry, which is defined by two nitrogen donors from two pyridine group in the axial positions, two oxygen donors from two coordinated water, and two oxygen donors from carboxyl groups in the equatorial plane (Figure S8 and S9). The 3D framework of **4** with hydrogen bonds is shown in Figure S10 in the Supporting Information.

Inhibitory Activity Against Jack Bean Urease

The compounds were evaluated for their inhibitory activities against jack bean urease (Table 4). It was found that compared with the reversible inhibitor acetohydroxamic acid (IC_{50} = 7.898 ± 0.898 μM), the synthesized ligand HL exhibited a weak ability to inhibit the jack bean urease (IC_{50} = 15.094 ± 2.218 μM), complex **2** showed IC_{50} = 6.868 ± 1.006 μM, and complex **3** and **4** showed no urease inhibitory activity. Notably, complex **1** displayed the best inhibitory activity against jack bean urease (IC_{50} = 4.052 ± 0.693 μM).

Table 4. Inhibition of jack bean urease by compounds HL, **1**–**4**, and acetohydroxamic acid.

Test compound	IC_{50} [μmol/L]
HL	15.094 ± 2.218
1	4.052 ± 0.693
2	6.868 ± 1.006
3	>100
4	>100
Acetohydroxamic acid[a]	7.898 ± 0.898

[a] Positive control.

Coordination modes of HL that appeared in complexes **1**–**4** are shown in Scheme 2. By docking simulations, the urease inhibitory activities and structure-activity relationships revealed that coordination to copper(II) ions resulted in improved inhibitory activity and that complex **1** is more potent than complex **2**, which indicated that mononuclear complex **1** was more effective than polymer **2**. This can be attributed to the free carboxyl groups that act as hydrogen-bond acceptors between complex **1** and urease, but the carbonyl oxygen is involved in the coordination in complex **2** (Scheme 2). Meanwhile, complex **2** coordinated to Cu^{II} ions exhibited better inhibitory ability than Zn^{II} and Fe^{II} ions as potential enzyme inhibitors, which in consistent with the inhibitory efficiency of metal ions towards urease.[18,19] The results indicated that inhibitory activities of metal complexes of HL depended not only on the structure but also on the central metal ions. The results intensified our interest in further structural modification of the present compounds as lead compounds for urease inhibitors.

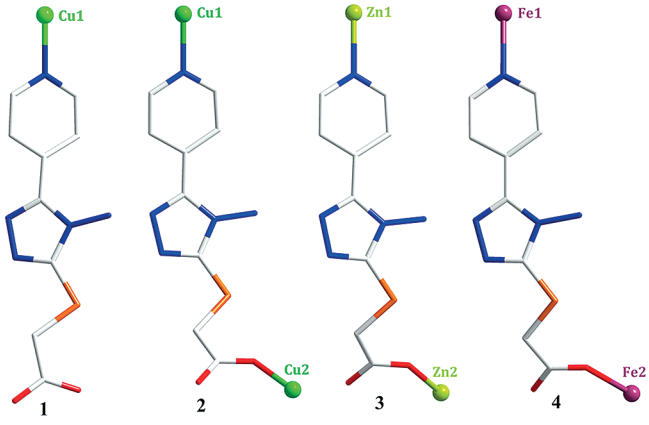

Scheme 2. Coordination modes of HL appearing in complexes **1**–**4**.

Kinetics of Urease Inhibition by Complexes 1 and 2

Kinetic studies showed that acetohydroxamic acid was a noncompetitive inhibitor, whereas the aryl hydroxamic acid derivatives were of a mixed type.[20] These paradoxical results encouraged us to study the inhibition mechanism of the obtained complexes. The mechanisms of inhibition of urease by two selected complexes **1** and **2** were investigated in kinetics inhibition with a Lineweaver–Burk plot. Double

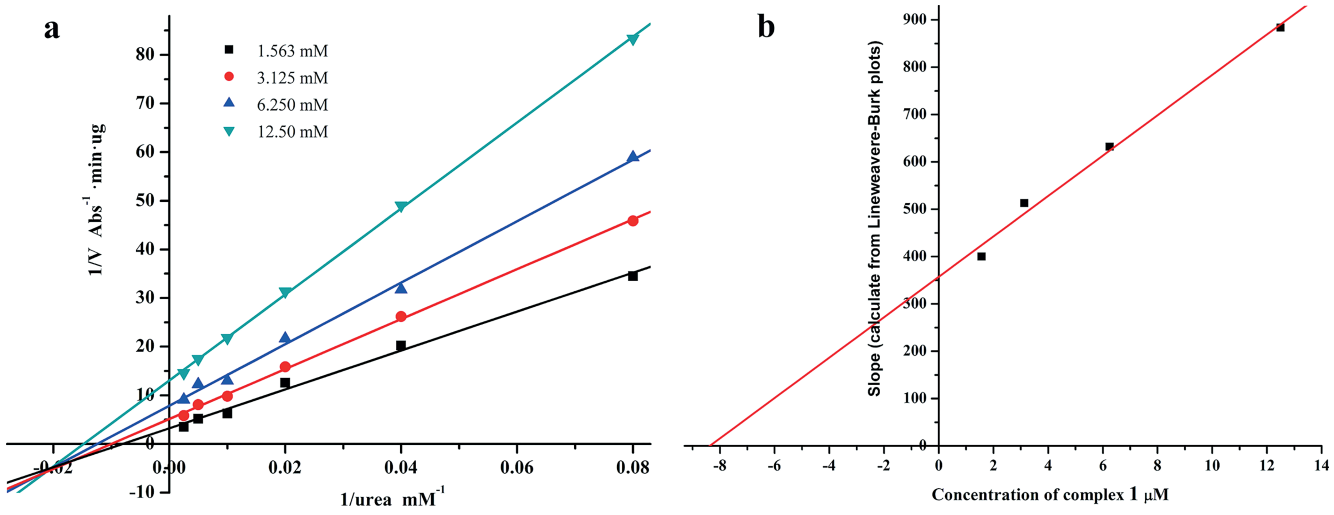

Figure 9. (a) Double-reciprocal Lineweaver–Burk plot of the inhibition of jack bean urease activity by complex **1**. (b) Plots of the slopes from the Lineweaver–Burk lines vs. different concentrations of complex **1**.

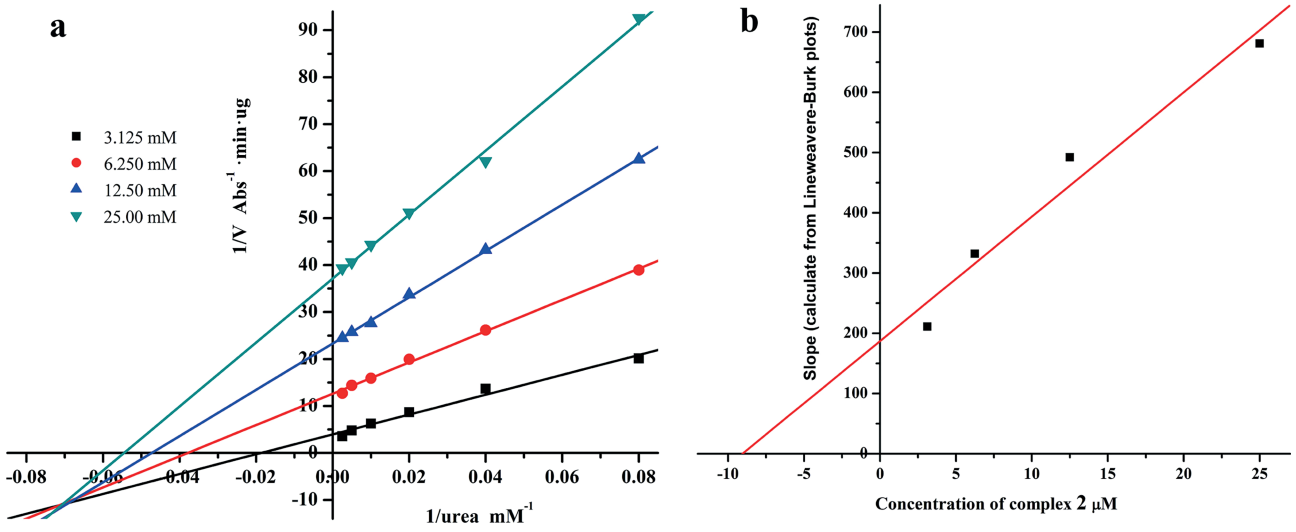

Figure 10. (a) Double-reciprocal Lineweaver–Burk plot of the inhibition of jack bean urease activity by complex **2**. (b) Plots of the slopes from the Lineweaver–Burk lines vs. different concentrations of complex **2**.

reciprocal plots of the data revealed that both **1** and **2** were mixed competitive inhibitors of urease instead of the expected competitive inhibitors with respect to the substrate urea. The K_i value was calculated from a plot of the slopes of the Lineweaver–Burk plot vs. the concentration of inhibitor. The obtained K_i values for complexes **1** and **2** were 8.375 and 9.056 μM, respectively (Figures 9 and 10).

Conclusions

We have reported the synthesis, crystal structures, molecular docking, and urease inhibitory activities of four new transition-metal complexes with 2-{[4-amino-3-(pyridin-4-yl)-4,5-dihydro-1*H*-1,2,4-triazol-5-yl]thio}acetic acid ligand. The molecular docking and the urease inhibitory activity studies of the complex against jack bean urease led to the development of valuable new urease inhibitors. The inhibitory activity tested in vitro against jack bean urease reveals that complex **1** displays the best inhibitory activity (IC_{50} = 4.052 ± 0.693 μM). The kinetics study reveals that complex **1** is a mixed-competitive inhibitor of urease with a K_i value of 8.375 μM. The computational predications showed good correlation with experimental data. The biological evaluation and mechanism study of complex **1** reveal that this complex will be of significant interest as a potent urease inhibitor candidate.

Experimental Section

Materials and Methods: Urease (from jack beans, type III, activity 34310 units/mg solid), HEPES (Ultra) buffer and urea (Molecular Biology Reagent) were purchased from Sigma–Aldrich Co. (St. Louis, MO, USA). All other chemicals and solvents were purchased from Aldrich and used as received. Distilled water was used

for all procedures. IR spectra were recorded with a FTIR Nicolet 5700 Spectrometer from 4000 to 400 cm^{-1}. The crystal data of trizole ligand and complexes were collected with a Bruker D8 VENTURE PHOTON diffractometer. Enzyme inhibitory activity was measured with a BioTek Synergy HT microplate reader.

Synthesis of the Ligand 2-{[4-Amino-3-(pyridin-4-yl)-4,5-dihydro-1*H*-1,2,4-triazol-5-yl]thio}acetic Acid (HL): Prepared by nucleophilic substitution reaction between chloroacetic acid and 4-amino-3-(pyridin-4-yl)-4,5-dihydro-1*H*-1,2,4-triazole-5-thiol, which was prepared through multistep reaction with isonicotinohydrazide by using the method of Reid and Heindel[21] with modifications.

Isonicotinohydrazide (13.7 g, 0.1 mol) reacted with carbon disulfide (9.04 mL, 0.15 mol) and potassium hydroxide (8.4 g, 0.15 mol) in absolute ethyl alcohol to give potassium dithiocarbazinate, which was then cyclized to 4-amino-3-(pyridin-4-yl)-4,5-dihydro-1*H*-1,2,4-triazole-5-thiol by reacting with hydrazine hydrate (10 mL, 0.16 mol), neutralized with hydrochloric acid to form the precipitate and then **HL** was synthesized with chloroacetic acid (14.25 g, 0.15 mol) and potassium hydroxide (8.4 g, 0.15 mol). The resulting mixture was heated to reflux for 12 h at 105 °C and, after cooling, the solvent was neutralized with hydrochloric acid to form a precipitate, which was isolated by filtration and purified by recrystallization from ethanol to give pure **HL** (15.891 g, 63%). $C_9H_{10}N_5O_2S$ (252.27): calcd. C 42.85, H 3.99, N 27.76; found C 42.84, H 4.00, N 27.76. IR (KBr): $\tilde{\nu}$ = 3464, 3295, 3184, 1645, 1578, 1445, 1388, 1224, 993, 727, 687, 652, 551 cm^{-1}.

$[Cu(L)_2(NH_3)_2(H_2O)_2]$ (1): Ligand **HL** (0.288 g, 1 mmol) was dissolved in a solvent mixture of methanol and *N*,*N*-dimethylformamide (1:1 v/v, 10 mL), and added to $Cu(CH_3COO)_2{\cdot}H_2O$ (0.200 g, 1 mmol) in methanol (5 mL). $NH_3{\cdot}H_2O$ (17%; 1 mL) was added and the resulting solution was stirred for 30 min at room temperature and then filtered. The filtrate was kept in air for about 7 d, forming crystals of **1** (0.295 g, 60%). $C_{18}H_{26}CuN_{12}O_6S_2$ (634.15): calcd. C 34.09, H 4.13, N 26.50; found C 34.08, H 4.14, N 26.51. IR (KBr): $\tilde{\nu}$ = 3284, 3178, 1617, 1591, 1450, 1360, 1231, 996, 740, 689, 603, 524 cm^{-1}.

$\{[Cu(L)_2(H_2O)_2]{\cdot}2H_2O\}_n$ (2): Ligand **HL** (0.288 g, 1 mmol) was dissolved in a solvent mixture of methanol and *N*,*N*-dimethylformamide (1:1 v/v, 10 mL), and added to $Cu(CH_3COO)_2{\cdot}H_2O$ (0.200 g, 1 mmol) in methanol (5 mL). The resulting solution was stirred for 15 min at room temperature and then filtered. The filtrate was kept in air for about 20 d, forming crystals of **2** (0.214 g, 43%). $C_{18}H_{20}CuN_{10}O_6S_2$ (600.09): calcd. C 36.03, H 3.36, N 23.34; found C 36.02, H 3.35, N 23.33. IR (KBr): $\tilde{\nu}$ = 3285, 3178, 1617, 1590, 1451, 1356, 1230, 995, 734, 688, 600, 523 cm^{-1}.

$\{[Zn(L)_2(H_2O)_2]{\cdot}2H_2O\}_n$ (3): Ligand **HL** (0.288 g, 1 mmol) was dissolved in a solvent mixture of methanol and *N*,*N*-dimethylformamide (1:1 v/v, 10 mL), and added to $Zn(CH_3COO)_2{\cdot}2H_2O$ (0.220 g, 1 mmol) in methanol (5 mL). The resulting solution was stirred for 15 min at room temperature and then filtered. The filtrate was kept in air for about 20 d, forming crystals of **3** (0.307 g, 63%). $C_{18}H_{20}N_{10}O_6S_2Zn$ (601.92): calcd. C 35.91, H 3.35, N 23.26; found C 35.92, H 3.34, N 23.27. IR (KBr): $\tilde{\nu}$ = 3311, 3191, 1624, 1458, 1381, 1228, 977, 730, 695, 593, 522 cm^{-1}.

Synthesis of $\{[Fe(L)_2(H_2O)_2]{\cdot}2H_2O\}_n$ (4): Ligand **HL** (0.288 g, 1 mmol) was dissolved in a solvent mixture of methanol and *N*,*N*-dimethylformamide (1:1 v/v, 10 mL), and added to a solution of $FeCl_2$ (0.126 g, 1 mmol) in methanol (5 mL). The resulting solution was stirred for 30 min at room temperature and then filtered. The filtrate was kept in air for about 40 d, forming crystals of **4** (0.302 g, 73%). $C_{18}H_{20}FeN_{10}O_6S_2$ (592.39): calcd. C 36.50, H 3.40, N 23.64; found C 36.49, H 3.39, N 23.65. IR (KBr): $\tilde{\nu}$ = 3291, 3184, 1609, 1588, 1445, 1365, 1243, 985, 742, 685, 607, 532 cm^{-1}.

Crystal Structure Determinations: X-ray crystallographic data were collected with a Bruker D8 VENTURE PHOTON diffractometer with graphite-monochromated Mo-K_α radiation (λ = 0.71073 Å) using the Genenic omega scan technique. The structure was solved by direct methods and refined on F^2 by full-matrix least-squares with Bruker's SHELXL-97 program.[22] All of the non-hydrogen atoms were refined anisotropically. All other hydrogen atoms were placed in geometrically ideal positions and constrained to ride on their parent atoms.

Molecular Docking: Molecular docking of the inhibitor with the 3D structure of jack bean urease (entry 3LA4 in the Protein Data Bank) was carried out by using the Autodock 4.2 program suite. The crystal structures of ligands were used in the docking protocol. The graphical user interface AutoDockTools was performed to setup every inhibitor–enzyme interaction; where all hydrogen atoms were added, Gasteiger charges were calculated and nonpolar hydrogen atoms were merged to carbon atoms. The Ni initial parameters were set as r = 1.170 Å, q = +2.0, and van der Waals well-depth of 0.100 kcal/mol.[23] The 3D structures of ligand molecule were saved in Mol2 format with the aid of the program MERCURY 3.0. The partial charges of Mol2 file were further modified by using the AutoDockTools package (version 1.5.4) so that the charges of the nonpolar hydrogen atoms would be assigned to the atom to which the hydrogen is attached. The choice of the flexible bonds in the ligands was in accordance with SP3 hybridization. The resulting file was saved as pdbqt file.

The A program was used to generate the docking input files. In all docking, a grid box size of $60 \times 60 \times 60$ pointing in x, y and z directions was built, the maps were centered on the Ni842 atom in the catalytic site of the protein. The nickel bridging hydroxide was retained in the calculations. A grid spacing of 0.508 Å and a distance-dependent function of the dielectric constant were used to calculate the energetic map. 50 runs were generated by using Lamarckian genetic algorithm searches. Default settings were used with an initial population of 50 randomly placed individuals, a maximum number of 2.5×10^6 energy evaluations, and a maximum number of 2.7×10^4 generations. A mutation rate of 0.02 and a crossover rate of 0.8 were chosen. The results of the most favorable free energy of binding were selected as the resultant complex structures. Usually, the first docking conformation of the docking results had the lowest energy, which indicated the stablest system and thus a likely binding interaction. The docking procedure of complex **1** with the enzyme active site of jack bean urease was performed as described.

Measurement of Jack Bean Urease Inhibitory Activity: The measurement of urease activity was carried out according to the procedure reported by Tanaka.[24] The assay mixture, containing 25 µL of jack bean urease (40 kU/L) (dissolved in distilled water) and 25 µL of the tested complexes of different concentrations (dissolved in DMSO/H_2O mixture (1:1 v/v)) was preincubated for 1 h at 37 °C in a 96-well assay plate. After preincubation, 200 µL of 100 mM HEPES (*N*-[2-hydroxyethyl] piperazine-*N*′-[2-ethanesulfonic acid]) buffer pH 6.8 containing 500 mM urea and 0.002% phenol red were added and incubated at 37 °C.[25] The reaction, which was measured with a microplate reader (570 nm), was required to produce enough ammonium carbonate to raise the pH of a HEPES buffer from 6.8 to 7.7, with the endpoint being determined by the color of phenol red indicator.[26]

Kinetics Study: Lineweaver–Burk plots of 1/absorbance vs. 1/urea were used to reveal the mechanism of inhibition. Urease inhibition

was measured by varying the concentration of urea in the presence of different concentrations of complexes **1** and **2**. Inhibitory constants (K_i) were determined as the intersection on the *x*-axis of the plots of the slopes vs. different concentrations of inhibitor, in which the slopes obtained from the Lineweaver–Burk lines. All experiments were conducted in triplicate.[27,28]

CCDC-1030213 (for H**L**), -1030214 (for **1**), -1030215 (for **2**), -1030216 (for **3**) and -1031065 (for **4**) contain the supplementary crystallographic data for this paper. These data can be obtained free of charge from The Cambridge Crystallographic Data Centre via www.ccdc.cam.ac.uk/data_request/cif.

Acknowledgments

This work was supported by the National Natural Science Foundation of China (NSFC) (grant number 21301108).

[1] B. Krajewska, *J. Mol. Catal. B* **2009**, *59*, 9–21.
[2] K. Stingl, K. Altendorf, E. P. Bakker, *Trends Microbiol.* **2002**, *10*, 70.
[3] S. Futagami, H. Takahashi, Y. Norose, K. Nagata, M. Kobayashi, T. Nomura, *Jpn. Soc. Gastroenterol.* **1994**, *91*, 2202.
[4] Zaheer-ul-Haq, M. A. Lodhi, S. Ahmad Nawaz, S. Iqbal, K. Mohammed Khan, B. M. Rode, R. Attaur, M. I. Choudhary, *Bioorg. Med. Chem.* **2008**, *16*, 3456.
[5] T. Tanaka, M. Kawase, S. Tani, *Life Sci.* **2003**, *73*, 2985–2990.
[6] Y. Katsura, S. Nishino, M. Ohno, K. Sakane, Y. Matsumoto, C. Morinaga, H. Ishikawa, H. Takasugi, *J. Med. Chem.* **1998**, *41*, 1777–1788.
[7] H. Q. Li, C. Xu, H. S. Li, L. Shi, Z. P. Xiao, H. L. Zhu, *ChemMedChem* **2007**, *2*, 1361–1369.
[8] Z. Amtul, M. Rasheed, M. I. Choudhary, S. Rosanna, K. M. Khan, Atta-ur-Rahman, *Biochem. Biophys. Res. Commun.* **2004**, *319*, 1053–1063.
[9] Y.-P. Xu, J. Qin, S.-M. Sun, T.-T. Liu, X.-L. Zhang, S.-S. Qian, H.-L. Zhu, *Inorg. Chim. Acta* **2014**, *423*, 469–476.
[10] K. Mahmood-ul-Hassan, S. Hameed, K. A. Yasin, T. Akhtar, K. M. Khan, *Monatsh. Chem.* **2010**, *141*, 479–484.
[11] D. M. Boghaei, S. Mohebi, *J. Mol. Catal. A* **2002**, *179*, 41.
[12] S. K. Dutta, D. B. Mc Conville, W. J. Youngs, M. Chaudhury, *Inorg. Chem.* **1997**, *36*, 2517.
[13] F. A. Devillanova, D. N. Sathyanarayana, G. Verani, *J. Heterocycl. Chem.* **2009**, *15*, 945–947.
[14] Y. Li, Z.-X. Wang, C.-G. Zhang, Q. Liu, L. Liu, *Inorg. Chem. Commun.* **2013**, *38*, 58–61.
[15] G. B. Deacon, R. J. Phillips, *Coord. Chem. Rev.* **1980**, *33*, 227.
[16] B. Morzyk-Ociepa, D. Michalska, A. Pietraszko, *THEOCHEM* **2004**, *688*, 79–86.
[17] A. D. Sample, R. L. LaDuca, *Inorg. Chim. Acta* **2014**, *421*, 18–25.
[18] C. Preininger, O. S. Wolfbeis, *Biosens. Bioelectron.* **1996**, *11*, 981.
[19] W. H. R. Shaw, D. N. Raval, *J. Am. Chem. Soc.* **1961**, *83*, 3184.
[20] G. R. Gale, L. M. Atkins, *Arch. Int. Pharmacod. Ther.* **1969**, *180*, 289–298.
[21] J. R. Reid, N. D. Heindel, *J. Heterocycl. Chem.* **1976**, *13*, 925–926.
[22] Bruker, *SMART* (version 5.63), *SAINT* (version 6.02), *SADABS* (version 2.03), Bruker AXS Inc, Madison, WI, USA, **2000**.
[23] F. Musiani, E. Arnofi, R. Casadio, S. Ciurli, *J. Biol. Inorg. Chem.* **2001**, *6*, 300–314.
[24] G. M. Sheldrick, *Acta Crystallogr., Sect. A* **2008**, *64*, 112–122.
[25] W. Zaborska, B. Krajewska, Z. Olech, *J. Enzyme Inhib. Med. Chem.* **2004**, *19*, 65–69.
[26] D. D. Van Slyke, R. M. Archibald, *J. Biol. Chem.* **1944**, *154*, 623–642.
[27] Z.-P. Xiao, Z.-Y. Peng, J.-J. Dong, J. He, H. Ouyang, Y.-T. Feng, C.-L. Lu, W.-Q. Lin, J.-X. Wang, Y.-P. Xiang, H.-L. Zhu, *Eur. J. Med. Chem.* **2013**, *63*, 685–695.
[28] Z.-P. Xiao, Z.-Y. Peng, J.-J. Dong, R.-C. Deng, X.-D. Wang, H. Ouyang, P. Yang, J. He, Y.-F. Wang, M. Zhu, X.-C. Peng, W.-X. Peng, X. H.-L. Zhu, *Eur. J. Med. Chem.* **2013**, *68*, 212–221.

Received: January 17, 2015
Published Online: March 20, 2015

